Characterization of particulate-bound polycyclic aromatic compounds (PACs) and their oxidations in heavy polluted atmosphere: A case study in urban Beijing, China during haze events

Li Juan Li [a,b,c], Steven Sai Hang Ho [a,b,d,*], Baihuan Feng [e,f], Hongbing Xu [e,f], Tong Wang [e,f], Rongshan Wu [e,f], Wei Huang [e,f], Linli Qu [g], Qiyuan Wang [a,b], Junji Cao [a,b,*]

[a] Key Lab of Aerosol Chemistry & Physics, Institute of Earth Environment, Chinese Academy of Sciences, Xi'an, China
[b] State Key Lab of Loess and Quaternary Geology (SKLLQG), Institute of Earth Environment, Chinese Academy of Sciences, Xi'an, China
[c] University of Chinese Academy of Sciences, Beijing, China
[d] Division of Atmospheric Sciences, Desert Research Institute, Reno, NV, USA
[e] Department of Occupational and Environmental Health, Peking University School of Public Health, Beijing, China
[f] Key Laboratory of Molecular Cardiovascular Sciences of Ministry of Education, Peking University, Beijing, China
[g] Hong Kong Premium Services and Research Laboratory, Lai Chi Kok, Hong Kong Special Administrative Region

HIGHLIGHTS

- PM$_{2.5}$, PAHs, OPAHs and other carbonaceous matters were monitored during a severe haze episode in Beijing in 2015.
- The average total quantified PAHs (ΣPAHs) and OPAHs (ΣOPAHs) during haze events were 10 times higher than those in clear days.
- A long period of haze is conducive to the accumulation and oxidation of contaminant.
- Formations of highly oxidized organic particulate matter favorably occur at RH > 60%.

GRAPHICAL ABSTRACT
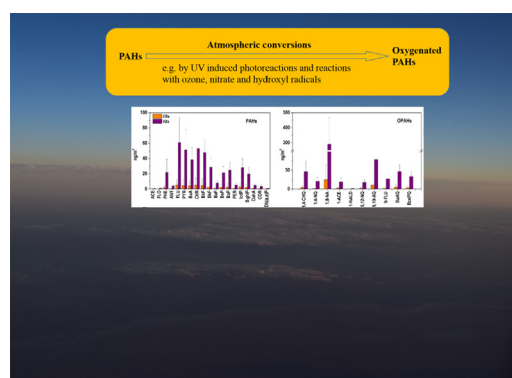
ARTICLE INFO

ABSTRACT

Characterizations on polycyclic aromatic compounds (PACs) during frequent haze periods have been conducted in an urban site of Beijing, China. Particulate polycyclic aromatic hydrocarbons (PAHs) and oxygenated-PAHs (OPAHs) and other carbonaceous matters were quantified. The average PM$_{2.5}$ during haze events (256.3 ± 103.7 μg/m^3) were one magnitude over than that of clear periods (CRs, 24.7 ± 27.7 μg/m^3).The average total quantified PAHs (ΣPAHs) and OPAHs (ΣOPAHs) during haze events were 423.9 ± 178.4 ng/m^3 and 581.4 ± 299.8 ng/m^3, respectively, which were approximately 10 times higher than those of 40.3 ± 68.2 ng/m^3 and 54.4 ± 82.4 ng/m^3 in clear days. Four-rings PAHs had the highest compositions. 1,8-Naphthalic anhydride (1,8-NA) is the most abundant OPAHs, accounted for 49.8% of $\sum$OPAHs, followed by 9,10-anthraquinone (9,10-AQ) (13.8%) and benzo(a)anthracene-7,12-dione (BaAQ) (8.31%). In haze events, the contents of 5- to 7-rings PAHs decreased by 2.32% compared with those of clear days, while lower molecular weight fractions of 3- and 4-rings PAHs increased. The relationships between PAHs, OPAHs and relative humidity (RH) were found to be exponential. High oxygenation rate (R$_o$) ratios of OPAH/PAH represents higher rates in secondary

---

* Corresponding authors at: Key Lab of Aerosol Chemistry & Physics, Institute of Earth Environment, Chinese Academy of Sciences, Xi'an, China.
E-mail addresses: stevenho@hkpsrl.org (S.S.H. Ho), cao@loess.llqg.ac.cn (J. Cao).

Oxygenation rate
Haze

formation or degradation and gas- particle conversion for each PAH or OPAH during the wintertime. Significant positive correlation between BeP and OPAHs ($r = 0.97$), combined with the results of photochemical aging and negatively correlation with O_3, suggest that secondary atmospheric reactions of PAHs played an important role in the burden of OPAHs.

1. Introduction

Atmospheric pollution has been being drawn high attention in Mainland of China due to its impacts on climate change and human health (Cai et al., 2017; Li et al., 2017a; Zhang, 2017). Haze event is typically defined as a visibility lower than 10 km and a mass concentration of airborne particulate matter with an aerodynamic diameter within 2.5 μm ($PM_{2.5}$) over 150 μg/m^3 (Cai et al., 2017; Guo et al., 2016; Ma et al., 2017; Zhang, 2017). Frequent haze events occurred in China, particularly in North China Plain. Researches demonstrated that discharges of primary local emission sources (Wu et al., 2014), immobile meteorological conditions for pollutant accumulations (Quan et al., 2014; Zheng et al., 2015), regional transport of pollutants (Quan et al., 2013) and secondary aerosol formation (Huang et al., 2014) are strongly associated with the formation of haze in the capital city of Beijing.

Chemicals such as trace elements, water-soluble inorganic compounds (WSIC), and carbonaceous species in airborne particulate of Beijing during haze days were harshly elevated in comparison to those of non-haze days (Gao et al., 2015; Tan et al., 2016; Zhang et al., 2016). Secondary organic carbon (SOC) was found to be an important fraction (Cao et al., 2003; Cao et al., 2004). However, variations on molecular levels for individual organic substances have been rarely reported between haze and non-haze periods. Particulate toxic compounds such as polycyclic aromatic hydrocarbons (PAHs) and their oxygenated forms (OPAHs) in $PM_{2.5}$ contribute to acute or potential long-term adverse health outcomes (Mumtaz and George, 1995; Walgraeve et al., 2010). These classes of compounds could be applied for source characterization and apportionment (Bandowe et al., 2014).

Atmospheric PAHs and OPAHs are formed natural sources (i e. volcanic eruptions and forest fires) and anthropogenic sources include various industrial processes, coal and wood burning, and fossil fuels combustion (Alam et al., 2013; Arnott, 2004; Ravindra et al., 2008). Besides direct formations, OPAHs, a neglected group of contaminants (Lundstedt et al., 2007), are produced via photochemical reactions and reactions with hydroxyl radicals, nitrate radicals and ozone (O_3) (Walgraeve et al., 2010). Airborne OPAH concentrations have been highly correlated with reactive oxygen species (ROS) formation, suggesting that oxidative stress is one of the toxicity mechanisms for aerosol-induced human health effects during PM episode or haze events (Sklorz et al., 2007).

Despite much effort on characterizing PM pollution, our knowledge on its sources contribution and evolution are still not fully understood. Atmospheric dynamic processes and atmospheric phenomena in hazy days are different from those in clear periods (Wang et al., 2014; Zhao et al., 2013). However, the related studies on polycyclic aromatic compounds (PACs) (i.e., PAHs and OPAHs) are still sparse. Beijing is the capital of China and has a population of >20 million. In this study, daily $PM_{2.5}$ were collected in urban site of Beijing in a heavy polluted month of December 2015. Chemical characterization for organic carbon (OC), element carbon (EC), PAHs, OPAHs, n-alkanes were conducted. Variations and relationship with meteorological parameters and other measured pollutants such as carbonic oxide (CO), nitric oxide (NO), nitrogen dioxide (NO_2), ammonia (NH_3), ozone (O_3), and $PM_{2.5}$ were also investigated. The main objectives are to: (1) characterize airborne organic $PM_{2.5}$ in different atmospheric pollution conditions; (2) investigate influences of photochemistry on the formation of OPAHs; and (3) identify possible sources contributed to the haze pollutions in

Beijing. This information is essential for establishing regulatory controls of these pollutants in Beijing.

2. Methodology

2.1. Site description

The sampling site (N39° 58′ 58″, E116°20′ 52″) was located on the roof of School of Public Health Building on the campus of Peking University Health Science Center (Beijing, China), approximately 20 m above the ground level. The location is close to the 4th Ring Road with heavy traffic. It is a representative of an urban area (Wehner et al., 2004; Wu et al., 2008). On daily basis, $PM_{2.5}$ were collected on quartz fiber filters (23×18 cm^2, Pall Life Science, Port Washington, NY, USA) using a high-volume air sampler (Thermo Fisher Scientific, Waltham, MA, USA) at a flow rate of 1 m^3/min for 24 h (from 08:00 am to the next day 07:59 am). Prior to the sampling, the filters were pre-fired in a furnace (780 °C, 3 h) to remove volatile substances and organic contaminants. A total of 35 daily samples (including one field blank per week) were collected from December 1, 2015 to December 31, 2015.

The masses of $PM_{2.5}$ were measured with gravimetric method. Each filter was weighed at least twice before and after sampling, which were being equilibrated in a controlled room at temperature of 22 ± 2 °C and relative humidity (RH) of 35–45%. The maximum differences between the repeated measurements were <15 and <20 μg for blank filters and loaded filters, respectively. To prevent any loss of volatiles, all samples were packed in pre-baked aluminum foils and stored in a freezer at −20 °C until chemical analyses. Barometric pressure, RH, wind speed and ambient temperature were measured in 1-minute interval with the use of an Automatic Weather Station (MAWS201, Vaisala, Vantaa, Finland) configured with visibility sensor (Vaisala Model PWD22) and RH probe (Vaisala Model QMH101). Briefly, commercial instruments from Thermo Fisher Scientific (TE), USA were used to measure O_3 (model 49I), CO (model 48I). Trace gases including sulfur dioxide (SO_2) and NO—NO_2—NO_X were measured every 1 min using trace gas analyzers (Ecotech Pty Ltd., Australia; Model 9850, Model 9841b), respectively. NH_3 was measured in real-time by a commercial ammonia analyzer (Picarro, G2103).

2.2. Chemical analyses

OC and EC were quantified from a 0.53 cm^2 punch of each sample. A DRI model 2001 carbon analyzer (Atmoslytic, Inc., Calabasas, CA, USA) following the IMPROVE_A thermal/optical reflectance (TOR) protocol was used for the carbon analyses (Chow et al., 2007; Chow et al., 1993; Ho et al., 2004). This produced data for four OC fractions (OC1, OC2, OC3, and OC4 at 140, 280, 480, and 580 °C in a helium [He] atmosphere, respectively); the pyrolyzed carbon fraction (OP, determined when reflected laser light attained its original intensity after oxygen [O_2] was added to the analysis atmosphere) and three EC fractions (EC1, EC2, and EC3 at 580, 740, and 840 °C, in a 2% O_2/98% He atmosphere, respectively). OC is defined as the sum of OC1, OC2, OC3, OC4, plus OP, and EC is defined as EC1, EC2, EC3 minus OP.

Organic compounds, including 19 PAHs, 10 OPAHs, and 25 n-alkanes (n-C_{16}-n-C_{40}), were quantified using in-injection port-thermal desorption/mass spectrometry (TD-GC/MS) method (Ho et al., 2008; Ho et al., 2011b; Ho and Yu, 2004). Briefly, aliquots of the filters

(0.53–2.63 cm^2) were cut into small pieces and inserted into TD tubes for analyses. The temperature of the injector port was at 50 °C before sample loading and then ramped to 275 °C for desorption in a splitless mode, while the GC oven temperature was kept at 30 °C. After the injector temperature reached the set point, the oven program started. The MSD was full scanned from 50 to 550 amu under electron impact ionization (EI) at a voltage of 70 eV and an ion source temperature of 230 °C. Identification was achieved by characteristic ion and retention times of the chromatographic peaks with those of authentic standards. Field blank filters were analyzed using the same procedures.

2.3. Quality assurance and control (QA/QC)

Detailed QA/QC procedures used in this study were documented elsewhere (Cao et al., 2003; Ho et al., 2008; Ho et al., 2011a; Li et al., 2018; Wang et al., 2016). Briefly, the aerosol sampler was checked and calibrated regularly during the sampling periods, and the field blank filters were collected to correct for backgrounds. The OC/EC analysis instrument was calibrated with known quantities of methane daily. Average blank filters were 1.72 and 0.09 μg/m^3 for OC and EC, respectively, and subtracted from each sample. The limit of detection (LOD) for EC and OC were <1.0 μg/m^3. Replicate analyses were done for each group of ten samples. The relative standard deviation (RSD) was <5% for Total Carbon (TC), and <10% for OC and EC.

PAHs, OPAHs and alkanes were quantified using the TD-GC/MS instrumentation. Chrysene-d$_{12}$ (98%, Sigma-Aldrich, Bellefonte, PA, USA), was added as internal standard (IS) for the PAHs, Benzophenone-D$_{10}$, Anthraquinone-D$_8$ (98%, J&K chemical Ltd., USA) for OPAHs, and n-tetracosane-d$_{50}$ (n-C$_{24}$D$_{50}$) (98%, Aldrich, Milwaukee, WI, USA) was used for the n-alkanes. A six-point calibration over a concentration range of 0.5–5.0 ng for each of the target compounds from a standard mixture (Sigma-Aldrich, Bellefonte, PA, USA) was established, and the correlation coefficients (R^2) for linear regressions of the calibration curves were >0.99. The relative standard deviation of the replicates for organic compounds was <15%. The limits of detection (LODs) and limit of quantity (LOQs) for the targeted organic species are listed in Table S1.

2.4. Data analysis

Secondary organic carbon (OC$_{sec}$) (Cao et al., 2004; Castro et al., 1999) is an index for characterization of pollution which was calculated as,

$$OC_{sec} = OC_{total} - (OC/EC)_{min} \times EC \qquad (1)$$

Molecular indicators of n-alkanes, such as carbon preference index (CPI) (Simoneit, 1999), odd-even predominance (OEP) (Wang et al., 2015), and plant wax n-alkanes ratio (WNA%) were adopted for pollution source-tracking and calculated by Eqs. (2)–(6):

$$CPI_1 = \sum C_{17} - C_{39} / \sum C_{18} - C_{40} \qquad (2)$$

$$CPI_2 = \sum C_{17} - C_{23} / \sum C_{18} - C_{24} \qquad (3)$$

$$CPI_3 = \sum C_{25} - C_{39} / \sum C_{26} - C_{40} \qquad (4)$$

$$OEP = [(C_n + 6C_{n+2} + C_{n+4})/(4C_{n+1} + C_{n+3})]^{(-1)^{n+1}} \qquad (5)$$

$$WNA\% = \frac{\sum[C_n - 0.5(C_{n+1} + C_{n-1})]}{\sum n - alkanes} \qquad (6)$$

3. Results and discussion

3.1. PM and other pollutants levels

We defined haze period (HZ) as continuous days with daily PM$_{2.5}$ mass concentrations over 150 μg/m^3, while the other days with PM$_{2.5}$ < 75 μg/m^3 are clear period (CR). Two typical HZ and CR were thus observed, including HZ$_I$ (December 6–9) and HZ$_{II}$ (December 20–25) and CR$_I$ (December 2–5) and CR$_{II}$ (December 14–16) respectively, along the study period.

Fig. 1 presents daily concentrations of PM$_{2.5}$, trace gases and meteorological conditions measured during the entire month of December in
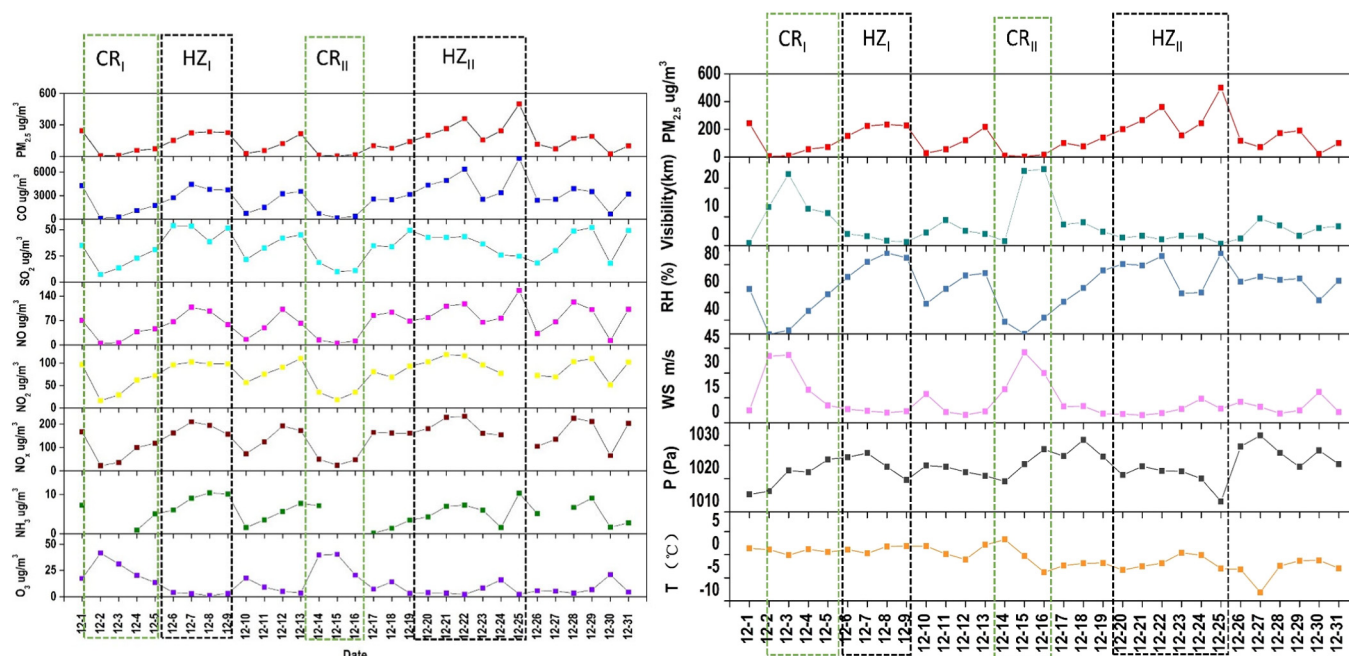

Fig. 1. Daily series of PM$_{2.5}$ concentration, trace gases and meteorological parameters. (CR$_I$, clear period I December 2–5; CR$_{II}$, clear period II December 14–16; HZ$_I$, haze period I December 6–9; HZ$_{II}$, haze period II December 20–25.)

Table 1
Summary the concentrations of target compounds in PM$_{2.5}$ in CRs and HZs ($n = 31$).

Compounds	CRI			CRII			HZI			HZII			Average concentration	
	Mean	SD	Range	Mean	SD	Range	Mean	SD	Range	Mean	SD	Range	Mean	SD
OC (μg/m3)	6.40	6.73	(0.32–13.74)	1.04	0.81	(0.38–1.94)	30.89	4.64	(24.98–35.08)	51.45	32.06	(19.76–110.09)	24.27	22.40
OC1	1.05	1.25	(0.03–2.70)	0.14	0.12	(0.04–0.27)	4.87	0.73	(4.17–5.90)	9.68	6.07	(3.1–20.09)	4.19	4.26
OC2	1.28	1.39	(0.06–2.90)	0.19	0.15	(0.07–0.36)	6.38	0.98	(5.09–7.26)	9.37	4.51	(4.06–17.18)	4.61	3.77
OC3	1.90	1.96	(0.11–3.92)	0.31	0.23	(0.13–0.57)	8.37	0.91	(7.27–9.46)	10.77	3.87	(5.55–16.38)	5.85	4.22
OC4	1.14	1.09	(0.10–2.10)	0.25	0.18	(0.12–0.46)	4.49	1.44	(2.76–6.27)	3.54	1.47	(1.79–5.96)	2.46	1.80
OP	1.03	1.12	(0.02–2.15)	0.15	0.13	(0.02–0.28)	6.78	3.95	(1.67–10.26)	18.09	18.57	(4.31–52.29)	7.15	10.32
EC (μg/m3)	3.49	3.80	(0.17–7.99)	0.48	0.36	(0.2–0.89)	17.70	3.31	(14.84–20.94)	23.55	7.04	(13.43–30.65)	12.00	8.84
EC1	4.18	4.58	(0.16–9.45)	0.51	0.41	(0.18–0.97)	22.59	8.17	(12.43–29.84)	40.64	22.24	(18.19–81.08)	11.21	8.46
EC2	0.31	0.30	(0.02–0.61)	0.11	0.08	(0.05–0.20)	1.83	1.51	(0.88–4.08)	0.77	0.32	(0.43–1.22)	0.68	0.73
EC3	0.03	0.04	(0.03–0.07)			–	0.07	0.06	(0.02–0.13)	0.22	0.10	(0.12–0.35)	0.11	0.10
PAHs (ng/m3)														
Acenaphthene (ACE)	0.09	0.08	(0.01–0.17)	0.02	0.01	(0.01–0.03)	0.50	0.30	(0.19–0.90)	0.51	0.25	(0.23–0.89)	0.27	0.24
Fluorene (FLO)	0.13	0.13	(0.02–0.26)	0.02	0.02	(0.01–0.04)	0.54	0.18	(0.32–0.73)	1.65	1.04	(0.48–3.4)	0.66	0.74
Phenanthrene (PHE)	2.85	2.91	(0.33–6.09)	0.37	0.21	(0.16–0.58)	8.95	2.19	(6.04–11.29)	30.34	17.64	(11.98–60.49)	12.47	13.16
Anthracene (ANT)	0.53	0.58	(0.04–1.26)	0.06	0.04	(0.04–0.10)	1.74	0.30	(1.45–2.07)	5.74	2.60	(2.63–9.27)	2.40	2.37
Fluoranthene (FLU)	8.43	9.84	(0.79–21.9)	0.82	0.64	(0.14–1.42)	37.36	7.89	(30.48–44.42)	76.42	34.92	(28.49–121.46)	34.62	30.58
Pyrene (PYR)	7.37	9.21	(0.58–20.38)	0.59	0.52	(0.03–1.07)	31.96	5.89	(27.46–39.85)	64.38	26.67	(25.28–89.35)	29.74	25.36
Benzo[a]anthracene (BaA)	6.80	9.57	(0.28–20.67)	0.42	0.10	(0.35–0.54)	28.40	10.97	(13.39–39.73)	45.14	14.98	(25.19–63.16)	22.52	17.54
Chrysene (CHR)	8.48	10.88	(0.47–23.77)	0.67	0.26	(0.47–0.96)	38.42	13.36	(20.29–51.97)	62.65	23.25	(32.5–87.65)	30.05	24.20
Benzo[b]fluoranthene (BbF)	7.93	10.35	(0.45–22.58)	0.62	0.21	(0.46–0.86)	38.84	14.25	(19.52–53.51)	53.59	16.95	(28.82–68.33)	27.44	20.78
Benzo[k]fluoranthene (BkF)	4.18	5.22	(0.26–11.43)	0.38	0.14	(0.27–0.53)	21.14	7.00	(11.76–28.39)	33.64	11.40	(19.36–45.59)	16.06	12.69
Benzo[a]fluoranthene (BaF)	1.40	2.01	(0.06–4.33)	0.09	0.02	(0.08–0.12)	6.11	2.50	(2.52–8.32)	8.97	3.84	(5.14–15.38)	4.64	3.64
Benzo[e]pyrene (BeP)	3.48	4.47	(0.21–9.77)	0.30	0.10	(0.22–0.41)	16.91	6.01	(9.10–23.61)	24.65	8.13	(13.5–32.49)	12.50	9.47
Benzo[a]pyrene (BaP)	4.21	5.86	(0.18–12.66)	0.27	0.06	(0.23–0.33)	18.79	7.76	(7.92–26.33)	28.64	9.80	(16.89–42.18)	14.61	11.14
Perylene (PER)	0.94	1.34	(0.04–2.89)	0.06	0.01	(0.05–0.07)	4.22	1.73	(1.87–6.05)	5.99	2.31	(3.70–9.30)	3.15	2.42
Indeno[1,2,3-cd]pyrene (IcdP)	4.43	5.72	(0.26–12.47)	0.36	0.10	(0.28–0.47)	21.64	7.65	(11.52–30.10)	32.32	12.27	(18.79–49.46)	16.58	12.60
Benzo[ghi]perylene (BghiP)	3.54	4.56	(0.20–9.95)	0.27	0.06	(0.24–0.34)	15.93	5.61	(8.84–22.45)	22.16	9.94	(14.01–37.67)	11.85	8.97
Dibenzo[a,h]anthracene (DahA)	0.83	1.09	(0.05–2.37)	0.06	0.01	(0.05–0.07)	3.69	1.51	(1.78–5.48)	5.63	1.81	(3.04–7.51)	2.89	2.16
Coronene (COR)	0.71	0.89	(0.04–1.94)	0.07	0.01	(0.06–0.08)	3.04	0.69	(2.34–3.74)	4.00	2.70	(1.89–8.84)	2.28	1.84
Dibenzo(a,e)pyrene (DaeP)	0.18	0.23	(0.01–0.51)	0.01	0.01	(0.01–0.01)	0.68	0.28	(0.43–0.92)	0.97	0.66	(0.41–2.12)	0.55	0.45
∑PAHs	66.50	84.60	(4.26–185.39)	5.45	2.44	(3.15–8.02)	298.87	79.61	(203.06–397.39)	507.39	180.56	(255.24–661.58)	245.27	192.70
OPAHs (ng/m^3)														

Table 1 (*continued*)

Compounds	CRI			CRII			HZI			HZII			Average concentration	
	Mean	SD	Range	Mean	SD	Range	Mean	SD	Range	Mean	SD	Range	Mean	SD
1,4-Naphthoquinone (1,4-NQ)	1.78	1.91	(0.18–4.11)	0.44	0.32	(0.15–0.78)	22.68	7.47	(15.17–33.01)	19.23	13.37	(3.88–40.44)	12.79	11.79
1-Naphthaldehyde (1-NALD)	0.23	0.23	(0.02–0.48)	0.04	0.03	(0.02–0.08)	1.08	0.97	(0.46–2.52)	1.09	0.45	(0.52–1.66)	0.65	0.55
1-Acenaphthenone (1-ACE)	3.44	4.21	(0.13–9.12)	0.60	0.54	(0.19–1.21)	15.91	12.05	(8.58–33.79)	21.07	8.30	(9.74–33.64)	10.48	8.83
9-Fluorenone (9-FLU)	3.04	2.72	(0.61–6.27)	0.75	0.54	(0.39–1.37)	25.89	33.38	(7.83–75.90)	28.29	18.48	(10.46–62.26)	13.93	17.07
9,10-Anthraquinone (9,10-AQ)	16.63	17.57	(0.26–37.81)	2.38	1.78	(0.84–4.33)	52.41	9.78	(40.21–63.84)	96.34	56.94	(45.33–197.37)	44.50	40.31
1,8-Naphthalic anhydride (1,8-NA)	40.84	47.42	(2.22–100.1)	3.42	2.90	(0.82–6.54)	193.16	69.18	(92.28–239.94)	355.40	202.48	(162.71–709.9)	163.13	156.03
Benzo(a)anthracene-7,12-dione (BaAQ)	7.36	9.39	(0.42–20.46)	0.80	0.82	(0.19–1.74)	35.09	12.48	(18.61–48.72)	54.12	20.19	(30.32–78.49)	27.25	21.18
1,4-Chrysenequinone (1,4-CHQ)	6.30	7.22	(0.51–15.73)	0.75	0.73	(0.17–1.57)	34.58	13.36	(19.98–50.88)	54.04	33.28	(23.51–107.96)	24.81	23.74
5,12-Naphthacenequinone (5,12-NQ)	2.76	3.55	(0.17–7.72)	0.25	0.25	(0.06–0.53)	14.54	6.57	(6.52–22.19)	20.10	8.21	(9.70–31.82)	10.16	8.24
6H-Benzo(c,d)pyrene-6-one (BcdPQ)	5.29	6.67	(0.31–14.55)	0.59	0.63	(0.13–1.31)	26.91	9.87	(13.99–38.01)	37.92	14.12	(23.77–56.88)	19.94	15.20
∑OPAHs	87.67	100.45	(5.84–216.33)	10.01	8.51	(2.96–19.46)	422.24	66.72	(223.63–608.8)	687.61	354.07	(319.94–1320.42)	327.62	290.44
n-Alkanes (ng/m3)														
Headecane (*n*-C16)	0.91	0.91	(0.12–2.04)	0.23	0.18	(0.05–0.41)	5.74	3.61	(1.44–10.28)	6.74	4.56	(3.68–14.84)	325.15	39.52
Heptadecane (*n*-C17)	1.22	1.19	(0.17–2.68)	0.35	0.24	(0.11–0.6)	7.20	5.08	(1.61–13.88)	8.19	4.26	(3.95–16.13)	367.17	41.87
Octadecane (*n*-C18)	1.33	1.27	(0.23–2.88)	0.39	0.24	(0.16–0.63)	7.41	6.35	(2.60–16.76)	9.91	4.94	(3.97–15.66)	397.15	44.30
Nonadecane (*n*-C19)	2.00	1.81	(0.49–4.42)	0.54	0.35	(0.24–0.93)	12.53	14.29	(4.08–33.85)	24.17	17.02	(5.47–52.59)	568.82	47.14
Icosane (*n*-C20)	4.84	4.91	(1.03–11.68)	1.04	0.65	(0.52–1.77)	24.57	21.24	(7.38–55.47)	61.89	47.56	(10.92–145.99)	1030.12	54.31
Heneicosane (*n*-C21)	10.18	11.51	(1.14–25.62)	1.57	1.16	(0.8–2.91)	41.59	14.16	(23.12–55.34)	101.04	64.28	(27.08–213.15)	1576.03	62.28
Docosane (*n*-C22)	15.01	17.53	(1.15–38.12)	1.62	1.06	(0.96–2.85)	66.82	14.14	(54.88–85.72)	135.65	72.65	(51.68–255.20)	2106.71	70.54
Tricosane (*n*-C23)	17.39	20.44	(1.23–44.3)	1.72	1.02	(1.05–2.9)	84.99	19.75	(60.14–108.36)	157.69	79.83	(63.82–283.82)	2441.05	77.33
Tetracosane (*n*-C24)	16.27	18.98	(1.11–40.96)	1.54	0.86	(0.99–2.53)	81.16	18.99	(56.36–102.65)	144.30	71.42	(60.89–259.16)	2299.94	75.23
Pentacosane (*n*-C25)	15.74	18.43	(1.10–39.94)	1.61	0.86	(0.96–2.58)	81.10	18.94	(57.98–104.37)	143.59	72.82	(58.78–259.57)	2303.60	77.14
heacosane(*n*-C26)	10.83	12.68	(0.69–27.39)	1.05	0.62	(0.59–1.75)	53.67	12.96	(38.88–70.37)	100.37	49.02	(45.33–179.48)	1706.02	69.65
Heptacosane (*n*-C27)	9.83	10.97	(1.03–24.17)	1.06	0.56	(0.55–1.66)	46.62	10.55	(33.61–58.86)	84.90	38.68	(38.74–140.62)	1527.58	69.06
Octacosane (*n*-C28)	4.42	5.12	(0.35–11.2)	0.48	0.28	(0.24–0.79)	24.76	5.11	(18.49–30.52)	40.34	17.27	(20.55–65.20)	948.61	68.32
Nonacosane (*n*-C29)	7.35	7.28	(1.22–16.51)	1.12	0.66	(0.41–1.73)	33.69	8.45	(23.56–43.33)	60.64	23.53	(30.24–83.88)	1241.23	71.18
Triacontane (*n*-C30)	2.79	3.10	(0.24–6.75)	0.34	0.21	(0.16–0.57)	16.16	3.09	(12.1–19.38)	28.75	11.97	(13.86–42.97)	803.75	73.26
Hentriacotane (*n*-C31)	3.50	3.17	(0.71–7.06)	0.70	0.38	(0.27–1.00)	14.89	2.68	(11.35–17.85)	27.84	9.25	(14.59–37.45)	823.72	75.54
Dotriacontane (*n*-C32)	1.29	1.36	(0.13–2.92)	0.17	0.10	(0.09–0.28)	6.44	1.16	(5.43–7.77)	12.73	4.92	(6.22–18.59)	621.12	78.72
Tritriactotane (*n*-C33)	1.36	1.33	(0.23–2.99)	0.21	0.10	(0.09–0.28)	5.67	1.17	(4.28–7.13)	11.70	4.73	(5.96–18.77)	624.37	81.23
Tetratriactane (*n*-C34)	0.86	0.91	(0.09–1.95)	0.08	0.04	(0.04–0.11)	3.40	0.56	(2.85–3.91)	7.53	4.21	(3.29–14.61)	577.55	83.99
Pentatriacontane (*n*-C35)	0.76	0.75	(0.08–1.53)	0.06	0.02	(0.05–0.08)	2.87	1.02	(1.73–4.09)	5.85	2.88	(2.84–10.45)	570.14	86.56
Hetatriacotane (*n*-C36)	0.30	0.35	(0.03–0.77)	0.03	0.01	(0.02–0.03)	1.16	0.29	(0.9–1.47)	2.77	1.56	(1.17–5.20)	541.87	89.25
Heptatriacotane (*n*-C37)	0.31	0.37	(0.03–0.83)	0.03	0.01	(0.02–0.04)	1.21	0.24	(1.00–1.56)	2.36	1.51	(0.90–4.99)	551.90	91.75
Ocatriacotane (*n*-C38)	0.25	0.30	(0.03–0.67)	0.02	0.01	(0.02–0.03)	1.09	0.40	(0.78–1.67)	2.12	1.06	(1.09–3.78)	563.19	94.24
Nonatriacotane (*n*-C39)	0.20	0.25	(0.02–0.54)	0.01	0.00	(0.01–0.01)	0.84	0.11	(0.7–0.96)	1.72	1.33	(0.51–3.94)	572.16	96.74
Tetracontane (*n*-C40)	0.15	0.18	(0.02–0.41)	0.01	0.00	(0.01–0.01)	0.58	0.19	(0.38–0.83)	1.29	1.04	(0.35–2.84)	578.85	99.25
∑*n*-Alkanes	129.11	144.84	(12.66–318.32)	15.98	9.37	(8.41–26.45)	626.20	93.02	(560.5–762.09)	1184.08	596.37	(485.64–2129.57)	510.25	476.86

CRI, clear period (December 2–5); CRII, clear period (December 14–16); HZI, haze period I (December 6–9); HZII, haze period II (December 20–25).

2015. The average daily PM$_{2.5}$ mass was 141.3 ± 114.9 μg/m^3, much higher than other polluted months in the same year (Zheng et al., 2015). In addition, the PM$_{2.5}$ mass during HZs (including HZ$_I$ and HZ$_{II}$) (256.3 ± 103.7 μg/m^3) were one magnitude over than that of CRs (including CR$_I$ and CR$_{II}$) (24.7 ± 27.7 μg/m^3). The maximum daily concentration of 500.3 μg/m^3 was found in December 25 during HZ$_{II}$, considerably exceeds the guideline value set by World Health Organization (WHO) for PM$_{2.5}$ of 25 μg/m^3 (WHO, 2006). Such high levels of PM$_{2.5}$ during HZs were likely due to stable synoptic meteorological conditions and increased use of coal and other fuels for winter heating (Ye et al., 2003). The lowest PM$_{2.5}$ level of 4.5 μg/m^3 was observed in December 15 during CR$_{II}$. In comparison, the average PM$_{2.5}$ mass during HZ$_{II}$ (287.7 ± 124.6 μg/m^3) was 1.4 times higher than that of HZ$_I$ (209.3 ± 38.5 μg/m^3).

For trace gases, the average concentrations in HZs were 2.3–6.5 times higher than those in CRs. Given that the utilization of new energy for heating, the concentration of SO$_2$ (33.5 ± 14.1 μg/m^3), emitted mainly from coal burning, was lower than that of NO$_2$ (78.5 ± 29.4 μg/m^3), which is mainly exhausted from fueled-vehicles (Hang et al., 2015). The concentrations of the trace gases displayed similar tendency as PM$_{2.5}$, except for O$_3$ (Fig. 1). The average O$_3$ concentration levels in CRs were 5.4 times higher than those in HZs. An evident negative spearman correlation ($r = -0.8$) between O$_3$ and PM$_{2.5}$ in winter is observed (Fig. S1). The O$_3$ levels crossing haze episodes remained at consistent low concentrations, attributed to low solar radiations (i.e., low temperatures and poor visibilities) and high NO$_2$ levels (Wang et al., 2012). The relationship between O$_3$ and PM$_{2.5}$ is complex. It is known that O$_3$, as an oxidant, can vary the concentration of free radicals in the atmosphere and thus impact the formation of secondary aerosols and the concentration of PM$_{2.5}$. Therefore, O$_3$ and NO$_2$ are both important contributing factors to PM$_{2.5}$ pollution, which can lead to the formation of haze (Xiao et al., 2011). General, while PM$_{2.5}$ loading was high, O$_3$ degraded atmospheric visibility but its concentration was reduced (EPA, 2009).

Average temperatures and thermal amplitudes (HZs: 0.5 ± 2.0 °C, CRs: 0.3 ± 2.1 °C) were almost constant during the sampling campaign. Significant fluctuation was observed for RHs (HZs: 78.6 ± 11.0%, CR:

39.6 ± 10.4%) and wind speeds (HZs: 7.5 ± 2.8 m/s, CRs: 29.1 ± 19.6 m/s). Meteorological conditions have strong impacts on the accumulation of air pollutants. RH was reported to be an important contributor to the visibility reduction (Quan et al., 2014). In the present study, the visibility decreased with increasing RH. When RHs increased from 30 to 88%, the visibility dropped from 26 km on December 15 (with highest wind speed of 42.2 m/s) to 0.6 km on December 25 (with lower wind speed of 8.5 m/s). During the 1-month observation period, there were a total of 14 days with visibility below 10 km, RH above 60%, and PM$_{2.5}$ mass concentration exceeded 150 μg/m^3. The lowest wind speed (4.5 m/s) was seen on December 21 with high PM$_{2.5}$ of 264.8 μg/m^3. Atmospheric pressure and amplitude slightly decreased during the haze occurrences and aggravation. The atmospheric pressure decreased from 1027.7 Pa on December 7 to 1019.6 Pa on December 9, and from 1023.7 Pa on December 21 to 1013.2 Pa on December 25.

3.2. Concentration variations of PAHs and OPAHs

Table 1 summarizes the concentrations of target organic component in PM$_{2.5}$ during the sampling periods. The statistical analysis showed that they all followed normal distribution (Kolmogorov–Smirnov test, $p > 0.05$). The average of total quantified PAHs concentration ($\sum$PAHs) in HZs (423.9 ± 178.4 ng/m^3) was ten times of that of CRs (40.3 ± 68.2 ng/m^3) on average. The $\sum$PAHs$_{HZII}$ (507.4 ± 180.5 ng/m^3) was 1.7 times higher than $\sum$PAHs$_{HZI}$ (298.9 ± 79.6 ng/m^3). Fluoranthene (FLU), chrysene (CHR), and pyrene (PYR) were the three most abundant PAHs, accounted for a sum of 36.5% and 36.6% of $\sum$PAHs in HZs and CRs, respectively (Fig. 2). Average BaP concentration was 24.7 ± 10.0 ng/m^3 in HZs, one magnitude of that of CRs and 21 times exceed the WHO guideline of 1.2 ng/m^3 (2017), suggesting that severe health risk in Beijing during the heavy polluted periods. The PAHs were classified according with the number of aromatic rings (i.e., 3–7) and their concentrations during CRs and HZs episodes are shown in Fig. 3. No significant percentage difference was observed. In CRs, the 4-rings PAHs contributed the most (46.7%), followed by the 5-rings (34.4%), the 6 rings (12.1%), the 3 rings
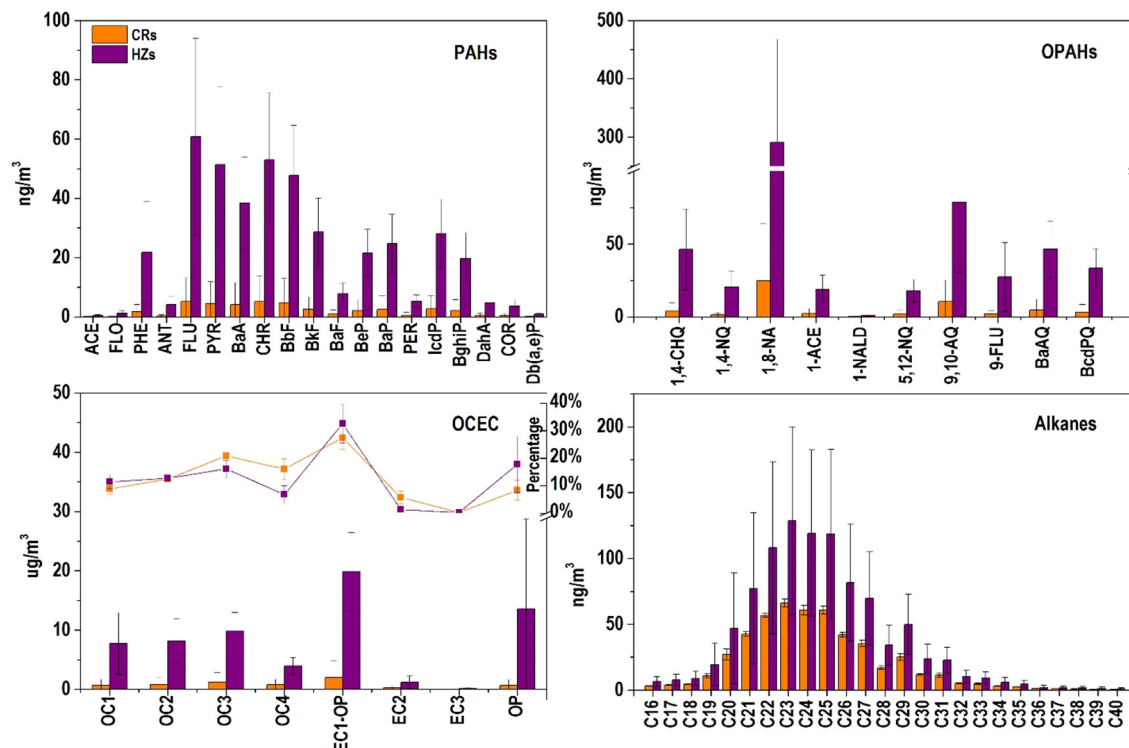

Fig. 2. Average and ranges of PAHs, OPAHs, OC, EC and Alkanes in PM$_{2.5}$ during CRs and HZs. (CRs, clear periods; HZs, haze periods).
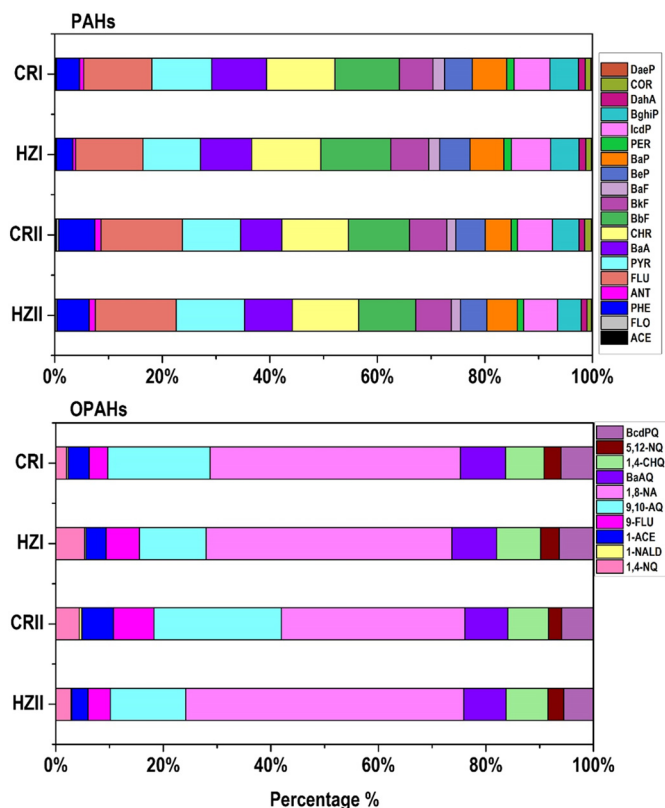
Fig. 3. The individual composition of PAHs and OPAHs during CRs and HZs. (CR$_I$, clear period I, December 2–5; CR$_{II}$, clear period II, December 14–16; HZ$_I$, haze period I, December 6–9; HZ$_{II}$, haze period II, December 20–25.)

(5.64%), and the 7 rings (1.13%). In HZs, similar trend was found while the compositions of 5- to 7-rings PAHs decreased by 2.32% but the 3–4 rings increased by 2.43%. This is attributed to the case that the concentrations of phenanthrene (PHE), FLU, and PYR were much higher in polluted days, which have been evidenced to be originated from coal combustions (Gao et al., 2011; Zhang et al., 2017). The finding is consistent with the fact that coal combustion was one of the pollutant source and contributed to atmospheric pollution during HZs (Li et al., 2017b).

The sum of OPAHs ($\sum$OPAHs) was 327.6 ± 290.4 ng/m^3 on average. The average $\sum$OPAHs in HZs (581.4 ± 299.8 ng/m^3) was ten times higher than that of CRs (54.4 ± 82.4 ng/m^3). Among the two haze events, the $\sum$OPAHs$_{HZII}$ (687.6 ± 354.1 ng/m^3) was 1.6 times higher than $\sum$OPAHs$_{HZI}$ (422.2 ± 66.7 ng/m^3). The PM$_{2.5}$-bound concentrations of OPAHs measured in wintertime were one or two magnitudes of the annual levels in Beijing in recent years, as well as other cities in China (Table S2). The average concentration of OPAHs during December in Beijing is the highest among the cities where the data are available.

Our measurements suggest that high levels of PM$_{2.5}$-bound OPAHs were present in the atmosphere of Beijing during winter. For individual compounds, 1,8-naphthalic anhydride (1,8-NA) is the most abundant OPAHs which accounted for 49.8% of $\sum$OPAHs, followed by 9,10-anthraquinone (9,10-AQ) (13.8%) and benzo(a)anthracene-7,12-dione (BaAQ) (8.31%). Relatively high concentrations of 1,8-NA could be

Table 2
Spearman correlation coefficients of OPAHs with parent PAHs.

	1-ACE	9FLO	ANTQ	BaAQ	1,4-CHQ	$\sum$OPAHs/$\sum$pPAHs
r	0.91	0.90	0.88	0.93	0.98	0.94
p	0.000	0.000	0.001	0.000	0.000	0.001

**Abbreviations for OPAHs are specified in the Table 1.

formed in the presence of the sunlight and low photochemical O$_3$ accumulation by the oxidation processes of several PAHs, such as acenaphthylene, acenaphthene (ACE) and even those with more than three rings like benzo[a]anthracene (BaA) based on the laboratory experiments (Kamens et al., 1989; Lee et al., 2001; Reyes et al., 1998; Sigman et al., 1996). Obvious proportion decrease of 9,10-AQ during HZs (HZ$_I$ 12.4% and HZ$_{II}$ 14.0%) was found compared of CRs (CR$_I$ 19.0% and CR$_{II}$ 23.7%) (Fig. 3). Good correlations between the individual pairs of parent PAHs (pPAHs) and their corresponding oxygenated forms (i.e., OPAH) (overall $r = 0.94$, Table 2) were observed, potentially suggesting that either OPAHs are formed from primary incomplete combustion or the significances of the secondary formation by radical reactions with pPAHs.

Fig. 3 compares the profiles of pPAHs and OPAHs in the Event I (i.e., CR$_I$ and HZ$_I$) and Event II (i.e., CR$_{II}$ and HZ$_{II}$). Interestingly, different patterns were shown between the two events. During Event I, the composition of middle molecular weights (MMW, 228 ≤ MW ≤ 252) PAHs (i.e., CHR, BbF, BkF, and BeP) in HZ$_I$ increased 2.43% from CR$_I$. However, the concentrations of MMW PAHs reversely dropped 1.72% in HZ$_{II}$ from CR$_{II}$ in Event II, while PYR and BaA increased by 3.01%. Meanwhile, the 5–7-rings PAHs in HZ$_{II}$ were 7.14% lower than that of HZ$_I$. The concentrations of other PAHs (i.e., FLO, PHE, ANT, FLU, and PYR) were 2.0–3.4 times higher in HZ$_{II}$ than HZ$_I$. For OPAHs, the concentrations of 1,4-NQ in HZ$_{II}$ were lower but 9,10-AQ and 1,8-NA were nearly twice of those in HZ$_{II}$. The contributions of high molecule weight OPAHs (MW ≥ 258) were more consistent. Lower contribution was found for low molecule weight OPAHs (MW ≤ 168) during HZ$_{II}$ than HZ$_I$.

3.3. Relationships of PACs with other atmospheric pollutants

The average OC and EC levels were 24.3 ± 22.4 and 12.0 ± 8.8 μg/m^3, respectively, in the entire month of December. The OC and EC were 4.1 ± 5.5 and 2.2 ± 3.1 μg/m^3, respectively, in CRs, whereas much higher values of 40.5 ± 26.5 and 19.9 ± 7.3 μg/m^3, respectively, were found in HZs. The average contributions of OC (CRs: 17.0%; HZs: 18.8%) and EC (CRs: 8.94%; HZs: 8.31%) to PM$_{2.5}$ were similar between the periods. Abundances of the thermal fractions differ by source type (Chow et al., 2004). Eight carbon fractions have been used for source appointment of carbonaceous (Cao et al., 2013; Kim et al., 2003). The average percentages for eight carbon fractions in CRs and HZs TC are shown in Fig. 2. The average abundances of OC1, OC2, OC3, OC4, EC1-OP, EC2, EC3 and OP during CRs (8.82%, 12.4%, 20.9%, 16.7%, 27.4%, 5.73%, 0.25% and 8.38%) were different from those during HZs (11.40%, 12.8%, 16.2%, 6.82%, 32.6%, 1.36%, 0.24%, and 17.8%), implying the different contributing sources carbonaceous aerosols throughout CRs and HZs. Closer inspection of the data shows that OC1 (volatile OC), EC1-OP percentages during the HZs were slightly higher than those during CRs. The percentages of OP during the HZs were nearly 2 times higher than those during CRs. OC3 (high temperature organic carbon) during the CRs was 20.9%, which was higher than that (16.2%) during HZs. The greater variability for OC contribution to TC among the carbonaceous fractions is due to more complex sources and most those leading to the formation of SOA (Cao et al., 2013).

The total carbonaceous aerosol (TCA) values, estimated by multiplying the amount of OC by a constant of 1.6 plus EC (Turpin and Lim, 2001), in HZs ranged from 45.0 to 205.9 μg/m^3, which were all higher than a range of 0.7 to 30.0 μg/m^3 in CRs. On average, the TCA accounted for 35.4% and 35.2% of PM$_{2.5}$ mass in CRs and HZs, respectively. Carbonaceous matter is an important component in PM$_{2.5}$. The average OC/EC ratios in HZs and CRs were similar (i.e., 2.0), which might reflect the combine contribution from coal combustion, motor-vehicle emission and biomass burning sources (Cao et al., 2005); however, the average OC/EC ratio in HZ$_{II}$ (2.1 for six days) was higher than that of HZ$_I$ (1.7 for four days), indicating that more secondary organics typically formed in persistent haze event (Chow et al., 1996). The average OC$_{sec}$ concentrations were 0.3 and 17.6 μg/m^3, respectively, in CRs and HZs, evidently

Table 3
Diagnostic ratios of n-alkanes and PAHs in PM$_{2.5}$ in CRs and HZs.

Indices of *n*-alkanes

	C$_{max}$	CPI$_1$	CPI$_2$	CPI$_3$	OEP	WNA%
CRs	C$_{23}$	1.29 ± 0.12	0.83 ± 0.03	2.25 ± 0.40	1.18 ± 0.06	0.14 ± 0.04
HZs	C$_{23}$	1.13 ± 0.03	0.80 ± 0.03	1.73 ± 0.05	1.13 ± 0.03	0.08 ± 0.02

Diagnostic ratios of PAH

	ANT / (PHE + ANT)	FLU / (FLU + PYR)	BaA / (BaA + CHR)	IcdP / (IcdP + BghiP)	BaP/BeP	PYR/BaP
CRs	0.11–0.17	0.51–0.58	0.36–0.47	0.55–0.59	0.81–0.95	1.60–3.20
HZs	0.13–0.19	0.52–0.57	0.34–0.45	0.57–0.65	0.87–1.29	1.30–4.10
Diagnostic Ratios	<0.1 Petrogenic sources >0.1 Pyrogenic sources	<0.4 Petrogenic sources 0.4–0.5 Fuel combustion >0.5 Wood, coal combustion	<0.2 Petrogenic 0.2–0.35 Petrogenic and combustion >0.35 Pyrogenic sources	<0.2 Petrogenic >0.2 Pyrogenic sources 0.2–0.5 Fuel combustion >0.5 Coal/biomass combustion	<0.6 Nontraffic sources >0.6 Traffic sources	~1 Gasoline ~10 Diesel
References	(Katsoyiannis et al., 2011)	(Torreroche et al., 2009)	(Akyüz and Çabuk, 2010)	(Yunker et al., 2002)	(Katsoyiannis et al., 2011)	(Ravindra et al., 2008)

CRs, clear period; HZs, haze period.
*Abbreviations for PAHs are specified in the Table 1.

accounted for 7.61% and 40.6%, respectively, of the total OC. Compared with those in HZ$_I$, higher percentages of OC1, OC2, and OC$_{sec}$ to TCA were also found in HZ$_{II}$ while the haze occurred for an extended period. Given that stable pollution sources in Beijing, both the chemical compositions of PM$_{2.5}$ and OC$_{sec}$ indicate that the SOA formations can be highly contributed to PM$_{2.5}$ in a long-term haze period. The finding was consistent with the study conducted by Huang et al. (2014).

Table S3 shows the correlation among PAHs, OC and EC. OC1, OC2, and EC1 show good correlations with typical PAHs, but the correlations become poor for OC3, OC4, EC2, EC3 and OP. It suggests OC1 and OC2 come from combustion source and vehicle emission. Most EC1 is pyrolysis char of OC, so good correlation is found between EC1 and PAHs. High molecular weight PAHs (COR and DaeP) show poorer correlations with OC and EC, which need further study.

The levels of homologue of C$_{16}$ to C$_{40}$ *n*-alkanes are illustrated in Fig. 2. The average total quantified *n*-alkanes concentration (Σ$_{n\text{-alkanes}}$) was 510.3 ± 476.9 ng/m^3. In HZs, the Σ$_{n\text{-alkanes}}$ ranged from 485.6 to 2129.6 ng/m^3, which were much higher than those in CRs, ranging from 8.4 to 318.3 ng/m^3. Table 3 summarizes C$_{max}$, CPI, OEP, and WNA % of the samples. The C$_{max}$ was at C$_{23}$ for all samples. The average CPI$_1$, CPI$_2$, and CPI$_3$ values were 1.3, 0.8, and 2.3 in CRs, and 1.1, 0.8, and 1.7 in HZs, respectively. The CPI$_1$ values were close to unity (CPI ≈ 1), indicating vehicular emissions and other anthropogenic activities during

Fig. 4. Ratio–ratio plot of BghiP and IcdP normalized by EC.

whole study (Bray and Evans, 1961). The petrogenic CPI$_2$ and biogenic CPI$_3$ values indicate that organic lipid from leaf epicuticular waxes is the predominant source for the heavier *n*-alkanes whereas large contributions from vehicle emission to lighter *n*-alkanes. CPI$_3$ in CRs is apparently higher than that in HZs, suggesting that higher contribution of biogenic source in CRs. Additional evidence for *n*-alkanes being anthropogenic-dominant is supported by the OEP values, which are 1.18 ± 0.06 and 1.13 ± 0.04 for CRs and HZs, respectively, that were close to unity. The average WAN% was significantly higher in CRs (14.2% ± 4.43%) than HZs (8.72% ± 1.62%). Our values were much lower than 18.5% measured in Qingdao, China in winter (Guo et al., 2003), indicating that lower influence from biogenic activities in Beijing particularly in HZs. All of these indices for *n*-alkanes support the dominant contributions from anthropogenic emissions.

A Spearman rank correlation analysis was performed to assess the relationships between PACs and trace gases and meteorological conditions. The results of correlation matrices are listed in Table S4. In fact, our results show that a proper negatively correlation ($R = -0.74$) exists between ΣPAH and O$_3$ concentrations, pointing out that O$_3$ formation in the urban atmosphere leads degradation of PAH compounds even in wintertime. This is corroborated with the estimated lifetimes of PAHs, ranging between 10 min and 24 h, in a polluted urban environment as far as their reaction with O$_3$ is concerned (Perraudin et al., 2007b). Concentrations of PAHs were well positively correlated with CO, NO, and NO$_2$ (Spearman coefficient: $R \geq 0.7$), except coronene (COR) and dibenzo(a,e)pyrene (DaeP). Low molecular weight (LMW) PAHs (i.e., FLO, PHE, ANT) were fairly correlated with SO$_2$ ($R \leq 0.6$), except chrysene (CHY). Such differences highlighted a disparity of sources may exist among individual PAHs. OPAHs were correlated with NO$_2$, NO, and CO ($R \geq 0.7$). The high correlations observed with primary pollutants from vehicular emissions (i.e., CO and NO) indicate that fuel combustion from traffic was the main source of OPAHs. However, OPAHs were negatively correlated with O$_3$. Besides, the Spearman coefficient of PAHs, OPAHs and RH were both high ($R \geq 0.7$) and their relationships were found to be exponential (Fig. S2). The incremental increased at high RH (≥60%) could enhance the formation of secondary components (Cheng et al., 2015).

3.4. Source identification and photochemical aging

PAHs are always emitted as a mixture, and the relative congener concentration ratios (diagnostic ratios) are supposed to be representative of a given emission source. Most diagnostic ratios involve pairs of PAHs congeners with the same molecular weight and similar
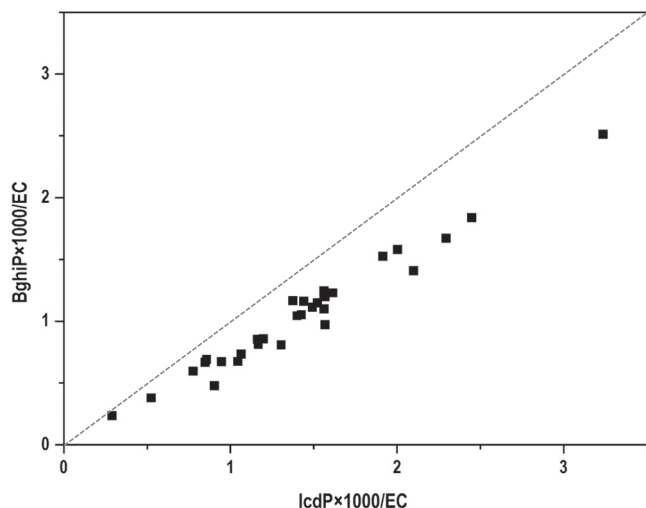
physicochemical properties, so they ought to undergo similar environmental fate processes.

Table 3 illustrates the results for six PAHs diagnostic ratios. Distinct results were observed. The values of ANT / (ANT + PHE) were mostly >0.1, pointing to the dominant contribution of pyrogenic sources (Katsoyiannis et al., 2011). Both of FLU / (FLU + PYR) and IcdP / (IcdP + BghiP) were >0.5, reflecting the influence of coal combustion and biomass burning. Contrarily, BaP/BeP ratios were >0.6 which indicates the relative abundance of traffic emission to the area (Zhang et al., 2017). The ratios of PYR/BaP, ranging from 1.3 to 4.1 and both below 10, were more consistent with a predominant gasoline combustion. Atmospheric processing rates could impact the distribution of isomers. Since ANT and BaA are more reactive in the atmosphere than their isomers aforementioned, the relatively low ratios of ANT / (ANT + PHE) and BaA / (BaA + CHR) may reflect the significances of photochemical processes and little local fresh emissions. To sum up, coal combustion, biomass burning and traffic emissions, were the main sources of $PM_{2.5}$ associated PAHs.

During atmospheric pollutant transportation, pPAHs are exposed to O_3, OH, NO_2 and other potential oxidants that degrade to various extents and thereby change their relative compositions (Brubaker and Hites, 1998; Esteve et al., 2006; Liu et al., 2006; Schauer et al., 2003). Both of PAHs and EC are known to be originated from combustion sources. However, while PAHs would decay in the atmosphere, EC is chemically stable. Therefore, photochemical degradation of PAHs would reduce the PAH-to-EC ratio in aged air compared with that from fresh emissions. In Fig. 4, low BghiP/EC vs ICdP/EC ratios were observed (below the zone of 1:1 line). It can be explained by either more extensive photochemical oxidation or source–source mixing, of which the mixing line distributed along the diagonal. The ratio of BaP/BeP could be also employed to illustrate whether the airs are fresh emitted or aged. It is well known that BeP has a relatively long atmospheric life time (i.e., higher persistence for chemical and/or biological degradation) (Katsoyiannis et al., 2011). While the ratios of BaP/BeP > 1 is indicative of fresh emission, those of lower than 1 represent the aged PAHs. In the present study, the BaP/BeP ratios varied from 0.81 to 1.29, manifesting that PAHs in the deposition samples had undergone aging processes.

The oxygenation rate (R_0) ratios of OPAH/PAH were 39.1 for 1-ACE/ACE, 1.28 for BaAQ/BaA, 21.4 for 9FLO/FLO, 20.8 for ANT/ANTQ and 0.81 for 1,4-CHQ/CHR (Table S5) on average which are generally higher than the ratios reported in fresh emission exhaust (Shen et al., 2015; Shen et al., 2012a; Shen et al., 2013a; Shen et al., 2013b) and other regions (Table S2). The results support that the higher oxygenation rates for secondary organic formation or degradation and gas-to-particle conversion for the PAHs or OPAHs during wintertime. High R_0 for ANT/ANTQ was in good agreement with results from reactivity studies of anthracene with O_3, where 9,10-anthraquinone and anthrone were accounted for the main compounds formed (Perraudin et al., 2007a). The atmosphere in sampling area experienced frequent pollutant accumulation in winter and was thus conducive to formation of SOA (Huang et al., 2014). The air reducants and oxidants might participate in the transformations of OPAHs with complex atmospheric reactions. Besides, a positive

correlation ($r = 0.97$) was seen between BeP and OPAHs. Referred to the results of R_0, BaP/BeP and negatively correlation with O_3, secondary atmospheric reaction of PAHs play an important role in the burden of OPAHs (Shen et al., 2013c; Walgraeve et al., 2010).

The correlation between trace gases, meteorological conditions and R_0 was performed (shown in Table S4). No statistical correlation was seen between 1-ACE/ACE, and ANT/ANTQ with trace gases nor with the meteorological conditions or ozone concentration. However, the air reducants and oxidants might participate in the transformations of OPAHs with complex atmospheric reactions. 9FLO/FLO had negative correlation with primary trace gases such as CO, SO_2, NO, NO_2, RH, and $PM_{2.5}$ (Table 4). However, it had positive correlation with O_3 and WS, suggesting that there was any remote transmission or increase of photochemical activity at higher O_3 concentrations. The ratios of BaAQ/BaA (1.0–1.7) and 1,4-CHQ/CHR (0.6–1.2) were more consistent than 1-ACE/ACE (13.5–65.1) and ANT/ANTQ (7.9–45.6) at different atmospheric conditions. Further researches are still needed to have better understanding on the effect of complex atmospheric processes and conditions for the formation or fate of the oxygenated PAHs.

4. Conclusion

The severe winter hazes were driven by stable synoptic meteorological conditions over Beijing, and not by an abrupt increase in anthropogenic emissions. The concentrations of carbonaceous matters in the atmosphere of Beijing winter were measured during the two sequent haze episodes in December 2015. The evolution of PAH and OPAHs pollution was found to coincide with the haze occurrence. The average concentrations of PACs were 10 times higher in HZs than CRs. The longer period of haze was conducive to the accumulation of contaminant and lead more SOA and oxidized products formations. The Spearman coefficient of PAHs, OPAHs and RH were relatively high ($R \geq 0.7$). High RH ($\geq 60\%$) could lead to the formation of highly oxidized organic PM.

Appendix A. Supplementary data

Supplementary data to this article can be found online at https://doi.org/10.1016/j.scitotenv.2019.01.078.

Table 4
The fitting results of 9FLO/FLO with trace gases and meteorological parameters.

	Fitting formula	R^2
CO	$y = -5.898\ln(x) + 25.101$	0.47
SO_2	$y = -9.449\ln(x) + 44.626$	0.31
NO	$y = -5.672\ln(x) + 42.766$	0.38
NO_2	$y = -11.71\ln(x) + 64.068$	0.46
NO_x	$y = -8.187\ln(x) + 57.502$	0.41
O_3	$y = 1.1638x + 16.454$	0.43
$PM_{2.5}$	$y = -4.746\ln(x) + 43.426$	0.45
WS	$y = 0.5999x + 14.628$	0.54
RH	$y = -0.3243x + 43.094$	0.37

References

Akyüz, M., Çabuk, H., 2010. Gas–particle partitioning and seasonal variation of polycyclic aromatic hydrocarbons in the atmosphere of Zonguldak, Turkey. Sci. Total Environ. 408, 5550–5558.

Alam, M.S., Delgado-Saborit, J.M., Stark, C., Harrison, R.M., 2013. Using atmospheric measurements of PAH and quinone compounds at roadside and urban background sites to assess sources and reactivity. Atmos. Environ. 77, 24–35.

Arnott, W.P., 2004. Phase and size distribution of polycyclic aromatic hydrocarbons in diesel and gasoline vehicle emissions. Environ. Sci. Technol. 38, 2557–2567.

Bandowe, B.A., Meusel, H., Huang, R.J., Ho, K., Cao, J., Hoffmann, T., Wilcke, W., 2014. $PM_{2.5}$-bound oxygenated PAHs, nitro-PAHs and parent-PAHs from the atmosphere of a Chinese megacity: seasonal variation, sources and cancer risk assessment. Sci. Total Environ. 473–474, 77–87.

Bray, E.E., Evans, E.D., 1961. Distribution of n-paraffins as a clue to recognition of source beds. Geochim. Cosmochim. Acta 22, 2–15.

Brubaker, W.W., Hites, R.A., 1998. OH reaction kinetics of polycyclic aromatic hydrocarbons and polychlorinated dibenzo-p-dioxins and dibenzofurans. J. Phys. Chem. A 102, 915–921.

Cai, W., Li, K., Liao, H., Wang, H., Wu, L., 2017. Weather conditions conducive to Beijing severe haze more frequent under climate change. Nat. Clim. Chang. 7, 257–262.

Cao, J.J., Lee, S.C., Ho, K.F., 2003. Characteristics of carbonaceous aerosol in Pearl River Delta region, China during 2001 winter period. Atmos. Environ. 37, 1451–1460.

Cao, J.J., Lee, S.C., Ho, K.F., Zou, S.C., Fung, K., Li, Y., Watson, J.G., Chow, J.C., 2004. Spatial and seasonal variations of atmospheric organic carbon and elemental carbon in Pearl River Delta region, China. Atmos. Environ. 38, 4447–4456.

Cao, J., Wu, F., Chow, J., Lee, S., Li, Y., Chen, S., An, Z., Fung, K., Watson, J., Zhu, C., 2005. Characterization and source apportionment of atmospheric organic and elemental carbon during fall and winter of 2003 in Xi'an, China. Atmos. Chem. Phys. 5, 3127–3137.

Cao, J.J., Zhu, C.S., Tie, X.X., Geng, F.M., Xu, H.M., Ho, S.S.H., Wang, G.H., Han, Y.M., Ho, K.F., 2013. Characteristics and sources of carbonaceous aerosols from Shanghai, China. Atmos. Chem. Phys. Discuss. 12, 803–817.

Castro, L.M., Pio, C.A., Harrison, R.M., Smith, D.J.T., 1999. Carbonaceous aerosol in urban and rural European atmospheres: estimation of secondary organic carbon concentrations. Atmos. Environ. 33, 2771–2781.

Cheng, Y., He, K.B., Du, Z.Y., Zheng, M., Duan, F.K., Ma, Y.L., 2015. Humidity plays an important role in the PM₂.₅ pollution in Beijing. Environ. Pollut. 197, 68–75.

Chow, J.C., Watson, J.G., Pritchett, L.C., Pierson, W.R., Frazier, C.A., Purcell, R.G., 1993. The dri thermal/optical reflectance carbon analysis system: description, evaluation and applications in U.S. air quality studies. Atmos. Environ. Part A 27, 1185–1201.

Chow, J.C., Watson, J.G., Lu, Z., Lowenthal, D.H., Frazier, C.A., Solomon, P.A., Thuillier, R.H., Magliano, K., 1996. Descriptive analysis of PM₂.₅ and PM₁₀ at regionally representative locations during SJVAQS/AUSPEX. Atmos. Environ. 30, 2079–2112.

Chow, J.C., Watson, J.G., Chen, L.-W.A., Arnott, W.P., Moosmüller, H., Fung, K., 2004. Equivalence of elemental carbon by thermal/optical reflectance and transmittance with different temperature protocols. Environ. Sci. Technol. 38, 4414–4422.

Chow, J.C., Watson, J.G., Chen, L.-W.A., Chang, M.-C.O., Robinson, N.F., Trimble, D.L., Kohl, S.D., 2007. The IMPROVE_A temperature protocol for thermal/optical carbon analysis: maintaining consistency with a long-term database. J. Air Waste Manage. Assoc. 57, 1014–1023.

EPA, U.S., 2009. Integrated Science Assessment for Particulate Matter (Final Report). US EPA - Environmental Protection Agency.

Esteve, W., Budzinski, H., Villenave, E., 2006. Relative rate constants for the heterogeneous reactions of NO and OH radicals with polycyclic aromatic hydrocarbons adsorbed on carbonaceous particles. Part 2: PAHs adsorbed on diesel particulate exhaust SRM 1650a. Atmos. Environ. 40, 201–211.

Gao, B., Yu, J.Z., Li, S.X., Ding, X., He, Q.F., Wang, X.M., 2011. Roadside and rooftop measurements of polycyclic aromatic hydrocarbons in PM₂.₅ in urban Guangzhou: evaluation of vehicular and regional combustion source contributions. Atmos. Environ. 45, 7184–7191.

Gao, J., Tian, H., Cheng, K., Lu, L., Zheng, M., Wang, S., Hao, J., Wang, K., Hua, S., Zhu, C., 2015. The variation of chemical characteristics of PM₂.₅ and PM₁₀ and formation causes during two haze pollution events in urban Beijing, China. Atmos. Environ. 107, 1–8.

Guo, Z.G., Sheng, L.F., Feng, J.L., Fang, M., 2003. Seasonal variation of solvent extractable organic compounds in the aerosols in Qingdao, China. Atmos. Environ. 37, 1825–1834.

Guo, L.C., Zhang, Y., Lin, H., Zeng, W., Liu, T., Xiao, J., Rutherford, S., You, J., Ma, W., 2016. The washout effects of rainfall on atmospheric particulate pollution in two Chinese cities. Environ. Pollut. 215, 195.

Hang, T.N., Kim, K.H., Park, C., 2015. Long-term trend of NO₂ in major urban areas of Korea and possible consequences for health. Atmos. Environ. 106, 347–357.

Ho, S.S.H., Yu, J.Z., 2004. In-injection port thermal desorption and subsequent gas chromatography–mass spectrometric analysis of polycyclic aromatic hydrocarbons and n-alkanes in atmospheric aerosol samples. J. Chromatogr. A 1059, 121–129.

Ho, K.F., Cao, J.J., Harrison, R.M., Lee, S.C., Bau, K.K., 2004. Indoor/outdoor relationships of organic carbon (OC) and elemental carbon (EC) in PM₂.₅ in roadside environment of Hong Kong. Atmos. Environ. 38, 6327–6335.

Ho, S.S.H., Yu, J.Z., Chow, J.C., Zielinska, B., Watson, J.G., Sit, E.H., Schauer, J.J., 2008. Evaluation of an in-injection port thermal desorption-gas chromatography/mass spectrometry method for analysis of non-polar organic compounds in ambient aerosol samples. J. Chromatogr. A 1200, 217–227.

Ho, S.S.H., Chow, J.C., Watson, J.G., Ng, L.P.T., Kwok, Y., Ho, K.F., 2011a. Precautions for in-injection port thermal desorption-gas chromatography/mass spectrometry (TD-GC/MS) as applied to aerosol filter samples. Atmos. Environ. 45 (7), 1491–1496.

Ho, S.S.H., Chow, J.C., Watson, J.G., Ting Ng, L.P., Kwok, Y., Ho, K.F., Cao, J., 2011b. Precautions for in-injection port thermal desorption-gas chromatography/mass spectrometry (TD-GC/MS) as applied to aerosol filter samples. Atmos. Environ. 45, 1491–1496.

Huang, R.J., Zhang, Y., Bozzetti, C., Ho, K.F., Cao, J.J., Han, Y., Daellenbach, K.R., Slowik, J.G., Platt, S.M., Canonaco, F., 2014. High secondary aerosol contribution to particulate pollution during haze events in China. Nature 514, 218–222.

Kamens, R.M., Karam, H., Guo, J., Perry, J.M., Stockburger, L., 1989. The behavior of oxygenated polycyclic aromatic hydrocarbons on atmospheric soot particles. Environ. Sci. Technol. 23, 801–806.

Katsoyiannis, A., Sweetman, A.J., Jones, K.C., 2011. PAH molecular diagnostic ratios applied to atmospheric sources: a critical evaluation using two decades of source inventory and air concentration data from the UK. Environ. Sci. Technol. 45, 8897–8906.

Kim, E., Larson, T.V., Hopke, P.K., Slaughter, C., Sheppard, L.E., Claiborn, C., 2003. Source identification of PM₂.₅ in an arid northwest U.S. City by positive matrix factorization. Atmos. Res. 66, 291–305.

Lee, B.D., Iso, M., Hosomi, M., 2001. Prediction of Fenton oxidation positions in polycyclic aromatic hydrocarbons by frontier electron density. Chemosphere 42, 431–435.

Li, L., Tan, Q., Zhang, Y., Feng, M., Qu, Y., An, J., Liu, X., 2017a. Characteristics and source apportionment of PM₂.₅ during persistent extreme haze events in Chengdu, southwest China. Environ. Pollut. 230, 718–729.

Li, H., Zhang, Q., Zhang, Q., Chen, C., Wang, L., Wei, Z., Zhou, S., Parworth, C., Zheng, B., Canonaco, F., 2017b. Wintertime aerosol chemistry and haze evolution in an extremely polluted city of North China Plain: significant contribution from coal and biomass combustions. EGU General Assembly Conference.

Li, L., Ho, S.S.H., Chow, J.C., Watson, J.G., Wang, L., Cao, J., 2018. Quantification of oxygenated polycyclic aromatic hydrocarbons in ambient aerosol samples using in-injection

port thermal desorption-gas chromatography/mass spectrometry: method exploration and validation. Int. J. Mass Spectrom. 433, 25–30.

Liu, Y., Sklorz, M., Schnelkreis, J., Orasche, J., Ferge, T., Kettrup, A., Zimmermann, R., 2006. Oxidant denuder sampling for analysis of polycyclic aromatic hydrocarbons and their oxygenated derivates in ambient aerosol: evaluation of sampling artefact. Chemosphere 62, 1889–1898.

Lundstedt, S., White, P.A., Lemieux, C.L., Lynes, K.D., Lambert, I.B., Öberg, L., Haglund, P., Tysklind, M., 2007. Sources, fate, and toxic hazards of oxygenated polycyclic aromatic hydrocarbons (PAHs) at PAH-contaminated sites. Ambio 36, 475.

Ma, Q., Wu, Y., Zhang, D., Wang, X., Xia, Y., Liu, X., Tian, P., Han, Z., Xia, X., Wang, Y., 2017. Roles of regional transport and heterogeneous reactions in the PM₂.₅ increase during winter haze episodes in Beijing. Sci. Total Environ. 599–600, 246–253.

Mumtaz, M.M., George, J.D., 1995. Toxicological Profile for Polycyclic Aromatic Hydrocarbons. Agency for Toxic Substances and Disease Registry, Atlanta, Ge., USA.

Perraudin, E., Budzinski, H., Villenave, E., 2007a. Identification and quantification of ozonation products of anthracene and phenanthrene adsorbed on silica particles. Atmos. Environ. 41, 6005–6017.

Perraudin, E., Budzinski, H., Villenave, E., 2007b. Kinetic study of the reactions of ozone with polycyclic aromatic hydrocarbons adsorbed on atmospheric model particles. J. Atmos. Chem. 56, 57–82.

Quan, J., Gao, Y., Zhang, Q., Tie, X., Cao, J., Han, S., Meng, J., PengfeiChen, DelongZhao, 2013. Evolution of planetary boundary layer under different weather conditions, and its impact on aerosol concentrations. Particuology 11, 34–40.

Quan, J., Tie, X., Zhang, Q., Liu, Q., Li, X., Gao, Y., Zhao, D., 2014. Characteristics of heavy aerosol pollution during the 2012–2013 winter in Beijing, China. Atmos. Environ. 88, 83–89.

Ravindra, K., Sokhi, R., Grieken, R.V., 2008. Atmospheric polycyclic aromatic hydrocarbons: source attribution, emission factors and regulation. Atmos. Environ. 42, 2895–2921.

Reyes, C., Sigman, M.E., Arce, R., Barbas, J.T., Dabestani, R., 1998. Photochemistry of acenaphthene at a silica gel/air interface. J. Photochem. Photobiol. A Chem. 112, 277–283.

Schauer, C., Niessner, R., Pöschl, U., 2003. Polycyclic aromatic hydrocarbons in urban air particulate matter: decadal and seasonal trends, chemical degradation, and sampling artifacts. Environ. Sci. Technol. 37, 2861–2868.

Shen, G., Tao, S., Wei, S., Zhang, Y., Wang, R., Wang, B., Wei, L.I., Shen, H., Huang, Y., Chen, Y., 2012a. Emissions of parent, nitro, and oxygenated polycyclic aromatic hydrocarbons from residential wood combustion in rural China. Environ. Sci. Technol. 46, 8123–8130.

Shen, G.F., Miao, X., Wei, S., Chen, Y.C., Wang, B., Rong, W., Yan, L., Shen, H.Z., Wei, L., Zhang, Y.Y., 2013a. Emissions of parent, nitrated, and oxygenated polycyclic aromatic hydrocarbons from indoor corn straw burning in normal and controlled combustion conditions. Acta Sci. Circumst. 25, 2072–2080.

Shen, G.F., Shu, T., Wei, S., Chen, Y.C., Zhang, Y.Y., Shen, H.Z., Ye, H., Dan, Z., Yuan, C.Y., Wang, H.C., 2013b. Field measurement of emission factors of PM, EC, OC, parent, nitro-, and oxy- polycyclic aromatic hydrocarbons for residential briquette, coal cake, and wood in rural Shanxi, China. Environ. Sci. Technol. 47, 2998–3005.

Shen, H., Huang, Y., Wang, R., Zhu, D., Li, W., Shen, G., Wang, B., Zhang, Y., Chen, Y., Lu, Y., 2013c. Global atmospheric emissions of polycyclic aromatic hydrocarbons from 1960 to 2008 and future predictions. Environ. Sci. Technol. 47, 6415–6424.

Shen, G., Chen, Y., Xue, C., Lin, N., Huang, Y., Shen, H., Wang, Y., Tongchao, L.I., Zhang, Y., Su, S., 2015. Pollutant emissions from improved coal- and wood-fuelled cookstoves in rural households. Environ. Sci. Technol. 49, 6590–6598.

Sigman, M.E., Chevis, E.A., Brown, A., Barbas, J.T., Dabestani, R., Burch, E.L., 1996. Enhanced photoreactivity of acenaphthylene in water: a product and mechanism study. J. Photochem. Photobiol. A Chem. 94, 149–155.

Simoneit, B.R., 1999. A review of biomarker compounds as source indicators and tracers for air pollution. Environ. Sci. Pollut. Res. Int. 6, 159–169.

Sklorz, M., Briedé, J.J., Schnellekreis, J., Liu, Y., Cyrys, J., de Kok, T.M., Zimmermann, R., 2007. Concentration of oxygenated polycyclic aromatic hydrocarbons and oxygen free radical formation from urban particulate matter. J. Toxicol. Environ. Health A 70, 1866–1869.

Tan, J., Duan, J., Zhen, N., He, K., Hao, J., 2016. Chemical characteristics and source of size-fractionated atmospheric particle in haze episode in Beijing. Atmos. Res. 167, 24–33.

Torreroche, R.J.D.L., Lee, W.Y., Camposdíaz, S.I., 2009. Soil-borne polycyclic aromatic hydrocarbons in El Paso, Texas: analysis of a potential problem in the United States/Mexico border region. J. Hazard. Mater. 163, 946–958.

Turpin, B.J., Lim, H.-J., 2001. Species contributions to PM₂.₅ mass concentrations: revisiting common assumptions for estimating organic mass. Aerosol Sci. Technol. 35, 602–610.

Walgraeve, C., Demeestere, K., Dewulf, J., Zimmermann, R., Langenhove, H.V., 2010. Oxygenated polycyclic aromatic hydrocarbons in atmospheric particulate matter: molecular characterization and occurrence. Atmos. Environ. 44, 1831–1846.

Wang, X., Shen, Z., Cao, J., Zhang, L., Liu, L., Li, J., Liu, S., Sun, Y., 2012. Characteristics of surface ozone at an urban site of Xi'an in northwest China. J. Environ. Monit. 14, 116–126.

Wang, Z.F., Jie, L., Zhe, W., Yang, W.Y., Xiao, T., Ge, B.Z., Yan, P.Z., Zhu, L.L., Chen, X.S., Chen, H.S., 2014. Modeling study of regional severe hazes over mid-eastern China in January 2013 and its implications on pollution prevention and control. Sci. China Earth Sci. 57, 3–13.

Wang, J., Ho, S.S.H., Cao, J., Huang, R., Zhou, J., Zhao, Y., Xu, H., Liu, S., Wang, G., Shen, Z., 2015. Characteristics and major sources of carbonaceous aerosols in PM₂.₅ from Sanya, China. Sci. Total Environ. 110, 530–531.

Wang, J., Ho, S.S.H., Huang, R., Gao, M., Liu, S., Zhao, S., Cao, J., Wang, G., Shen, Z., Han, Y., 2016. Characterization of parent and oxygenated-polycyclic aromatic hydrocarbons (PAHs) in Xi'an, China during heating period: An investigation of spatial distribution and transformation. Chemosphere 159, 367.

Wehner, B., Wiedensohler, A., Tuch, T.M., Wu, Z.J., Hu, M., Slanina, J., Kiang, C.S., 2004. Variability of the aerosol number size distribution in Beijing, China: new particle formation, dust storms, and high continental background. Geophys. Res. Lett. 31, 217–244.

WHO, 2006. Guidelines for Particulate Matter, Ozone, Nitrogen Dioxide and Sulfur Dioxide: Global Update 2005: Summary of Risk Assessment.

WHO, 2017. Evolution of WHO air quality guidelines: past, present and future. WHO Regional Office for Europe, Copenhagen.

Wu, Z., Hu, M., Lin, P., Liu, S., Wehner, B., Wiedensohler, A., 2008. Particle number size distribution in the urban atmosphere of Beijing, China. Atmos. Environ. 42, 7967–7980.

Wu, Y., Liu, Y., Zheng, X., Zhang, S., Song, S., Li, J., Hao, J., 2014. Characterization and source apportionment of particulate PAHs in the roadside environment in Beijing. Sci. Total Environ. 470–471, 76–83.

Xiao, Z.M., Zhang, Y.F., Hong, S.M., Bi, X.H., Jiao, L., Feng, Y.C., Wang, Y.Q., 2011. Estimation of the main factors influencing haze, based on a long-term monitoring campaign in Hangzhou, China. Aerosol Air Qual. Res. 11, 873–882.

Ye, B., Ji, X., Yang, H., Yao, X., Chan, C.K., Cadle, S.H., Chan, T., Mulawa, P.A., 2003. Concentration and chemical composition of PM$_{2.5}$ in Shanghai for a 1-year period. Atmos. Environ. 37, 499–510.

Yunker, M.B., Macdonald, R.W., Vingarzan, R., Mitchell, R.H., Goyette, D., Sylvestre, S., 2002. PAHs in the Fraser River basin: a critical appraisal of PAH ratios as indicators of PAH source and composition. Org. Geochem. 33, 489–515.

Zhang, R., 2017. Atmospheric science: warming boosts air pollution. Nat. Clim. Chang. 7, 238–239.

Zhang, Y., Huang, W., Cai, T., Fang, D., Wang, Y., Song, J., Hu, M., Zhang, Y., 2016. Concentrations and chemical compositions of fine particles (PM$_{2.5}$) during haze and non-haze days in Beijing. Atmos. Res. 174-175, 62–69.

Zhang, Y., Schauer, J.J., Zhang, Y., Zeng, L., Wei, Y., Liu, Y., Shao, M., 2017. Correction to characteristics of particulate carbon emissions from real-world Chinese coal combustion. Environ. Sci. Technol. 42, 5068–5073.

Zhao, X.J., Zhao, P.S., Xu, J., Meng, W., 2013. Analysis of a winter regional haze event and its formation mechanism in the North China plain. Atmos. Chem. Phys. 13, 5685–5696.

Zheng, G., Su, H., Zhang, Q., Cheng, Y., He, K., 2015. Exploring the severe winter haze in Beijing: the impact of synoptic weather, regional transport and heterogeneous reactions. Atmos. Chem. Phys. 15, 2969–2983.